Chapter 2
First Section: Putative CSF biomarkers of Alzheimer's disease based on the novel concept of generic protein misfolding and proteotoxicity: the PRAMA cohort

1. Demographic characteristics and classical CSF biomarker distributions of the PRAMA cohort

29 patients with diagnosis of AD (AD cases) and 23 patients with diagnosis of other diseases affecting the CNS (non-AD cases) have participated to this study, for a total of 52 patients. CSF samples were collected from all patients and treated as reported in *Chapter 1- Materials and Methods*. Table 2.1 reports the mean demographic characteristics of both groups, as well as their mean values of the classical CSF biomarkers ($A\beta_{42}$/ $A\beta_{40}$ ratio and levels of t-tau and p-tau), the percentages of patients with the ε4 allele of the *APOE* gene and the mean scores of MMSE tests. Table 2.1. reports the individual values of the same parameters for all 52 patients, one by one.

The total protein concentrations of the 23 non-AD and 29 AD cases, measured using the Bradford assay, were found to have a good degree of variability, as they ranged from ca. 0.2 to ca. 1.0 mg/ml in both groups (Figure 2.1 A), in agreement with previous analyses (Dufour-Rainfray *et al*. 2013). Their mean values were 0.44 ± 0.21 and 0.44 ± 0.19, respectively, indicating similar distributions in the two groups.

The classical CSF biomarkers, namely the $A\beta_{42}$/ $A\beta_{40}$ ratio, t-tau and p-tau levels, measured with established clinical protocols as described in *Chapter 1 – Materials and Methods*, also showed a good degree of variability, but their mean values were significantly different in the two groups: 0.089 ± 0.022 and 0.053 ±

Liliana Napolitano, liliana98.napolitano@gmail.com, 0009-0004-3087-286X

Referee List (DOI 10.36253/fup_referee_list)
FUP Best Practice in Scholarly Publishing (DOI 10.36253/fup_best_practice)

Liliana Napolitano, First Section*: Putative CSF biomarkers of Alzheimer's disease based on the novel concept of generic protein misfolding and proteotoxicity: the PRAMA cohort*, © Author(s), CC BY 4.0, DOI 10.36253/979-12-215-0993-9.04, in Liliana Napolitano, *A multidisciplinary approach for the early diagnosis of Alzheimer's disease and potential therapeutic applications*, pp. 65-77, 2026, published by Firenze University Press, ISBN 979-12-215-0993-9, DOI 10.36253/979-12-215-0993-9

Book References DOI 10.36253/979-12-215-0993-9.references

0.020 for the $A\beta_{42}/A\beta_{40}$ ratio ($p<0.0001$), 306 ± 246 and 763 ± 315 for t-tau ($p<0.0001$) and 43 ± 41 and 127 ± 61 for p-tau ($p<0.0001$), in non-AD and AD groups, respectively (Figure 2.1 B,C,D). The scatter plots of $A\beta_{42}/A\beta_{40}$ *versus* t-tau and $A\beta_{42}/A\beta_{40}$ *versus* p-tau, with the optimized thresholds (t^*) derived from optimization of the Youden's indexes of the two parameters (horizontal and vertical lines, respectively), show a good separation between non-AD and AD cases, with the latter having, on average, high values of t-tau and p-tau and low values of $A\beta_{42}/A\beta_{40}$, as expected (Figure 2.2 A,C).

In particular, the three quadrants above the t^* value for t-tau (or p-tau) and below the t^* value for $A\beta_{42}/A\beta_{40}$ contain mainly AD cases and few non-AD cases, whereas the remining quadrant contains a disproportionate amount of non-AD versus AD cases ($p<0.0001$ for both Fisher's exact test and Chi-square test, for both scatter plots). The AUC in the ROC curve were found to be 0.865, 0.889 and 0.887 (>0.5) for $A\beta_{42}/A\beta_{40}$, t- tau and p-tau, respectively (Figure 2.2 B,D). Overall, the good separation of non-AD and AD cases using classical CSF biomarkers in scatter plots indicate that the two groups are good representatives of non-AD and AD cases, respectively.

2. Non-AD and AD CSFs have similar circular dichroism spectra and parameters

In order to search CSF biomarkers independent of specific protein levels and using spectroscopic methods, we started our analysis with far-UV CD spectroscopy. Far-UV CD spectra recorded for the various CSF samples displayed a good degree of variability in non-normalized mean residue ellipticity (θ), as shown for five representative non-AD and five representative AD CSF samples (Figure 2.3 A). The θ values at the wavelength of 222 nm (θ_{222}) for all 52 CSF samples ranged from ca. - 22 to ca. -162 mdeg (cell 0.1 cm) in both groups (Figure 2.3 B). Their mean values were -59 ± 36 and -57 ± 33 in non-AD and AD cases, indicating the absence of a significant difference ($p = 0.84$).

In both non-AD and AD cases, θ_{222} correlated with protein concentration measured with the Bradford assay (Figure 2.4 A,B) and with the high tension (HT) signal at 222 nm (HT_{222}), which is also a correlate of total protein concentration (Figure 2.4 C,D). This indicates that the variability of CD spectra resulted from the variability in protein concentration. That HT_{222} is a correlate of the concentration of CSF proteins rather than other compounds present in the CSF samples and possibly contributing to the optical absorption, is shown by the correlation between HT_{222} and protein concentration measured with the Bradford assay in the two groups of patients (Figure 2.4 E,F).

In all CD spectra, negative peaks at ca. 208 and 222 nm were observed indicating that the spectra are dominated by proteins with substantial α-helical structure (Figure 2.3 A). This occurs because the all-α human serum albumin (HSA) is by far the most abundant protein in CSF and only one of the first ten most abundant proteins of the CSF is all-β, with the other nine being either mixed α

/β or all-α proteins (Lardinois *et al*. 2014). When other CD parameters were evaluated, including wavelength of the first or second peak, θ at any given wavelength, ratios of θ at two given wavelengths, θ normalized for protein concentration, etc., no significant differences were found between the non-AD and AD groups.

3. Non-AD and AD CSFs have different wavelengths of maximum fluorescence emission

We then compared the various CSF samples by recording their intrinsic tryptophan fluorescence spectra, which also appeared to be highly variable in terms of overall fluorescence intensity, as shown for the same representative five non-AD and five AD CSF samples (Figure 2.3 C). The values of fluorescence intensity at the wavelength of maximum emission (λ_{max}) ranged from ca. 160 a.u. to ca. 1200 a.u. in both groups and their mean values were 595 ± 260 and 502 ± 150 in non-AD and AD cases (Figure 2.3 D), indicating the absence of a significant difference, although a trend seems to be present ($p = 0.11$, Student *t* test). Subtle variations of the λ_{max} value was found in the various fluorescence spectra (Figure 2.3 E). In particular, the λ_{max} values ranged from 338 to 344 nm in non-AD cases and from 338 to 349 nm in AD cases, with a few AD cases having very high λ_{max} values, producing an extended tail out of the Gaussian distribution (Figure 2.3 E). The mean values in the two groups were 340.9 ± 1.4 nm and 341.9 ± 2.7 nm, respectively (Figure 2.3 E), indicating the absence of a significant difference, although a trend seems again to be present ($p = 0.11$). The λmax of the intrinsic fluorescence spectrum of a protein correlate positively with the solvent exposure of its tryptophan residues, which are hydrophobic and generally buried within the hydrophobic cores of native proteins (with lower λmax values), but become solvent exposed in case of partial or total unfolding or misfolding (with higher λ_{max} values). The anomalously high λ_{max} values of some AD cases indicate that, on average, their CSF proteins have a higher extent of partially unfolded or misfolded proteins.

4. Non-AD and AD CSFs have different quantities of protein aggregates

Size distributions of the particles present in CSF samples were acquired with dynamic light scattering (DLS), as shown here for the same representative five non-AD and five AD cases (Figure 2.5 A,B). In both cases, a peak of small species having an apparent hydrodynamic diameter (D_h) of ca. 10 nm is evident, which arises from the dominant largest CSF proteins, such as HSA. However, large species arising from protein aggregates are also present in both groups, all having D_h values around or higher than 100 nm (Figure 2.5 A,B). The light scattering intensity (*LSI*) arising from small species (D_h~ 10 nm) and large species (D_h> 30 nm) is higher in non-AD and AD cases, respectively, indicating a larger proportion of protein aggregates in the latter group (Figure 2.5 A,B). This

difference remains evident when considering all 23 non-AD and 29 AD cases, with large species accounting for 57 ± 20% and 67 ± 25% of *LSI* in the two groups, respectively (Figure 2.5 C). The difference is not yet significant but indicates again a trend ($p = 0.12$).

To interpret these data, we need to consider that *LSI* scales with the square and sixth power of the mass and *Dh* of the particles present in the sample, respectively. Therefore, the percentage of aggregate-derived *LSI* is a large overestimate of the percent population of these species in a CSF sample. When the size distributions are converted into light scattering volume (%) rather than *LSI* (%), the smaller species become dominant (data not shown). However, it is just because of this relationship between LSI and *Dh* that the DLS technique is very sensitive to protein aggregates, allowing to unravel and compare CSF samples with subtle differences in aggregate populations.

Another relevant DLS parameter is the light scattering count rate (LSCR), which corresponds to the total number of photons scattered by the sample per time unit, in units of kilocounts per second (kcps), and correlating again with the size of CSF particles. The LSCR ranges from ca. 30 to ca. 650 kcps and from ca. 50 to ca. 1200 Kcps in the two groups, respectively, with means of 248 ± 206 and 322 ± 258 kcps, respectively (Figure 2.5 D). This difference is not significant, however ($p = 0.27$).

5. Non-AD and AD CSFs have different abilities to destabilize cell membranes.

It is well known that protein aggregates have the ability to bind to and destabilize biological membranes and, when added to the extracellular medium of cell cultures, they destabilize the cell membrane and cause an influx of Ca^{2+} ions from the medium into the cytosol (Bigi *et al*. 2020; Cascella *et al.* 2021; Fani *et al*. 2021; Fani *et al*. 2022; Bigi *et al.* 2023a). We therefore tested the 23 non-AD and 29 AD CSF samples to cultured SH- SY5Y neuroblastoma cells by adding them to the extracellular medium (1:1) and measuring the intracellular Ca^{2+} levels after 5 h, using the Fluo-4 AM probe and confocal fluorescence microscopy. Cells left untreated (negative control) and treated with 1 μM ionomycin for 2 h (positive control) had very low (100%) and very high (677%) intracellular Ca^{2+} levels (Figure 2.6 A). Cells treated with CSF samples had variable increases of intracellular Ca^{2+} levels, as shown for the representative five non-AD and five AD samples (Figure 2.6 A). The Ca^{2+} levels ranged from ca. 110% to ca. 250% in non-AD cases (with the exception of one outlier sample) and from ca. 140 to ca. 340% in AD patients, relative to untreated cells (Figure 2.6 B). The mean values in the two groups were 181 ± 54% and 229 ± 53%, respectively, relative to untreated cells (Figure 2.6 B) and the difference is highly significant ($p = 0.0021$).

We also evaluated the ability of the various CSF samples to impair mitochondrial function of SH-SY5Y cells using the MTT reduction test, which measures the ability of the mitochondria to reduce the tetrazolium due MTT to formazan after 24 h of treatment (Cascella *et al*. 2021; Fani *et al.* 2021; Cascella *et al*. 2022; Bigi *et al*. 2023a). Both non- AD and AD cases caused, on average, small

decreases of MTT reduction relative to untreated cells, with values from ca. 77 to ca. 103% and from ca. 79 to ca. 105% in the two groups, respectively (Figure 2.6 C). However, the two groups were found to behave similarly with values of 93.5 ± 6.3% and 92.0 ± 7.7%, respectively ($p = 0.45$). The MTT reduction assay may fail to reveal differences between the two groups relative to the Ca^{2+} assay, both because of its lower sensitivity and because mitochondrial dysfunction is a downstream process in a complex cascade of events that start with aggregate-induced membrane destabilization as its earliest event when aggregates are added extracellularly (Kayed *et al*. 2004; Demuro *et al*. 2005; Zampagni *et al*. 2011; Cascella *et al*. 2021; Fani *et al*. 2022). For this reason, the Ca^{2+} assay distinguishes directly and with higher sensitivity the presence of potentially toxic aggregates in the CSF samples.

6. Evidence for fluorescence, DLS, and toxicity parameters as potential AD biomarkers

The analysis presented so far indicates that AD CSF samples are characterized by higher values of (i) λ_{max} values in intrinsic tryptophan fluorescence spectra, (ii) *LSI* from large protein species in the DLS analysis and (iii) cytosolic Ca^{2+} ion levels induced in cultured cells. This finding has a rationale in the presence of higher amounts of (i) misfolded proteins exposing tryptophan residues, (ii) large protein particles and (iii) misfolded protein oligomers inducing Ca^{2+} dyshomeostasis in cells, respectively.

The scatter plot of *LSI* from large protein species versus λ_{max} with the thresholds (t^*) derived from optimization of the Youden's indexes of the two parameters (horizontal and vertical lines, respectively), indicates a separation between non-AD and AD cases (Figure 2.7 A). The three quadrants above one or both t^* values contain mainly AD cases and few non-AD cases, whereas the only quadrant below both t^* values contains a disproportionate amount of non-AD versus AD cases ($p = 0.011$, Fisher's exact test; $p = 0.0075$, Chi-square test). A diagnosis of AD based on the CSF parameters occupying one of the three quadrants above at least one t^* value has a modest sensitivity but fairly good specificity (medium probability of false negatives but low probability of false positives). The AUC values in the ROC curve were found to be 0.648 and 0.560 (>0.5) for *LSI* and λ_{max}, respectively, indicating a fairly good accuracy of a test based on the two parameters separately (Figure 2.7 B).

The scatter plot for intracellular Ca^{2+} levels versus λ_{max} indicates a better separation between non-AD and AD cases (Figure 2.7 C). The three quadrants above one or both t^* values contain nearly all AD cases but also a non-negligible amount of non-AD cases, whereas the quadrant below both t^* values contain very few AD cases and a large amount of non-AD cases ($p = 0.0016$, Fisher's exact test; $p = 0.0009$, Chi-square test). Consequently, a diagnosis of AD based on these two CSF parameters occupying one of the three quadrants above at least one t^* value has a high sensitivity and medium specificity (very low probability

of false negatives but medium probability of false positives). The AUC values in the ROC curve were found to be 0.780 and 0.560 (>0.5) for Ca^{2+} levels and λ_{max}, respectively, indicating again a good accuracy of a test based on the two parameters separately (Figure 2.7 D).

The scatter plot for intracellular Ca^{2+} levels versus *LSI* also indicates a good separation between non-AD and AD cases (Figure 2.7 E), similarly to the previous analysis ($p = 0.0006$, Fisher's exact test; $p = 0.0003$, Chi-square test), reporting again a high sensitivity and medium specificity. The AUC values in the ROC curve were found to be 0.780 and 0.648 (>0.5) for Ca^{2+} levels and *LSI*, respectively, indicating again a good accuracy of a test based on the two parameters separately (Figure 2.7 F).

7. Comparison between novel and classical biomarkers.

As a next step in our analysis, we combined three classical and well-established CSF biomarkers ($A\beta_{42}/A\beta_{40}$ ratio, t-tau levels and p-tau levels) with the three novel putative biomarkers identified here (intrinsic fluorescence λ_{max}, *LSI* from large protein species in DLS and cytosolic Ca^{2+} levels in cells). The scatter plots for all possible pairs are shown in Figure 2.8. The scatter plots for each of three novel biomarkers versus $A\beta_{42}/A\beta_{40}$ ratio all show a good separation between non-AD and AD cases (Figure 2.8 A,C), with non-AD and AD cases crowding the bottom-right and three remaining quadrants, respectively ($p<0.0001$, Fisher's exact and Chi-square tests for the plot with λ_{max}; $p<0.0001$, Fisher's exact and Chi-square tests for the plot with *LSI*; $p = 0.001$, Fisher's exact test, and $p = 0.0007$, Chi-square test for the plot with Ca^{2+} levels). The scatter plots for each of three novel biomarkers versus either T-tau levels (Figure 2.8 D,F) or P-tau levels (Figure 2.8 G,I) also show a good separation with non-AD and AD cases occupying, in all cases, the bottom-left and three remaining quadrants, respectively ($p<0.0001$, Fisher's exact and Chi-square tests for λ_{max}; $p<0.0001$, Fisher's exact and Chi-square tests for *LSI*; $p = 0.0004$, Fisher's exact test, and $p = 0.0003$, Chi-square test for Ca^{2+} levels). In all nine scatter plots we obtained a similarly high sensitivity but a higher specificity relative to the analyses obtained with pairs of novel biomarkers, indicating that combined analyses with established and novel biomarkers improve the overall accuracy.

Since the Ca^{2+} levels and the three classical biomarkers ($A\beta_{42}/A\beta_{40}$ ratio and levels of t-tau and p-tau) separate very well the two AD and non-AD populations, the best level of diagnosis in terms of both sensitivity and specificity is achieved when considering AD cases only in one quadrant, which is the top-left for Ca^{2+} levels versus $A\beta_{42}/A\beta_{40}$ ratio (Figure 2.8 C) and the top-right for Ca^{2+} levels versus t-tau (Figure 2.8 F) and p-tau (Figure 2.8 I). The number of false positives and false negatives are only 1-3 out of 23 cases and 2-3 out of 29 cases, respectively ($p<0.0001$ with both statistical tests). The comparison between scatter plots built with pairs of classical biomarkers (Figure 2.2 A,C) and mixed classical and novel biomarkers (Figure 2.8) indicate good separations with $p<0.0001$ in all

cases, using both the Fisher's exact and Chi-square tests. This observation legitimates the use of the three novel CSF parameters analyzed here for AD diagnosis.

The comparison between scatter plots built solely with pairs of novel biomarkers (Figure 2.7) and those built solely with classical biomarkers (Figure 2.2 A,C) also indicate good separations in all cases, provided Ca^{2+} levels is utilized as one of the novel biomarkers ($p<0.002$ in all cases, using both statistical tests). The scatter plot using intrinsic fluorescence λ_{max} and *LSI* from large species yields the least satisfactory performance.

8. Chapter 2: figures and tables

	ApoE ε4+ [a]	Age at CSF collection	p-tau (pg/ml)	t-tau (pg/ml)	$A\beta_{42}$ (pg/ml)	$A\beta_{42}$ /$A\beta_{40}$	MMSE score [b]
Non - AD	18.2% (n=22)	71.8 ± 7.0 (n=21)	42.6 ± 40.5 (n=23)	305.7 ± 246.0 (n= 23)	708.0 ± 389.1 (n=23)	0.089 ± 0.022 (n=23)	26.4 ± 4.3 (n=5)
AD	40.7% (n=27)	70.2 ± 7.3 (n=29)	126.9 ± 60.6 (n=29)	763.1 ± 315.0 (n=29)	675.0 ± 295.9 (n=29)	0.053 ± 0.020 (n=29)	19.7 ± 5.7 (n=25)

Table 2.1 - Mean genetic, demographic and clinical characteristics and biomarkers distribution of the studied non-AD and AD patients. [a] All patients underwent *APOE* genotyping: *APOE* genotype was coded as *APOE* ε4- (no *APOE* ε4alleles) and *APOE* ε4+ (presence of one or two *APOE* ε4 alleles). The column reports the percentage of *APOE* ε4+ genotype and the number of patients analysed (n). [b] The MMSE score ranges for any patient from 0 to 30, with 30 indicating high brain performance. The n value of non-AD cases is low because there was no clinical indication to perform a MMSE test in many cases.

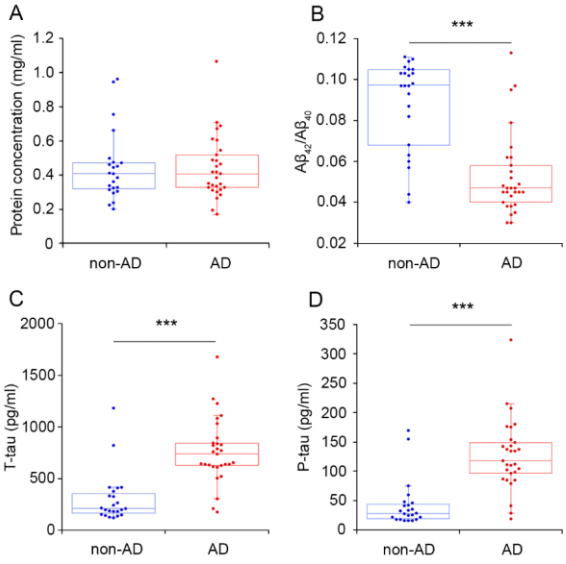

Figure 2.1 - Box plots reporting the protein concentration determined with the Bradford assay (A), the $A\beta_{42}/A\beta_{40}$ ratio (B), T-tau levels (C) and P-tau levels (D) in all CSF samples

of non-AD and AD patients. The boxes, horizontal lines, whiskers and individual dots have the same meaning as in Figure 2a. The two populations were compared with the Student *t* test in all plots (*** $p < 0.001$).

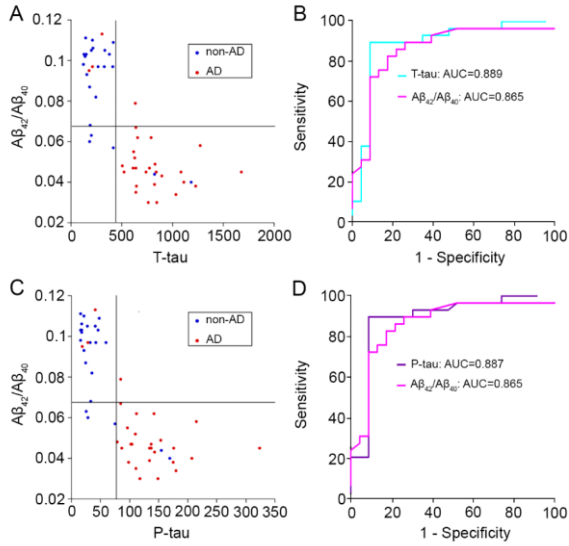

Figure 2.2 - (A,C) Scatter plots for the $A\beta_{42}/A\beta_{40}$ ratio versus T-tau (A) and P-tau (C). (B,D) ROC curves of the $A\beta_{42}/A\beta_{40}$ ratio and T-tau (B) and of the $A\beta_{42}/ A\beta_{40}$ ratio and P-tau (D). AUC values are indicated for each parameter. Non-AD (blue) and AD (red) CSF samples categorized to occupy the top-left quadrant or the remaining three quadrants provide a good separation between non-AD and AD patients.

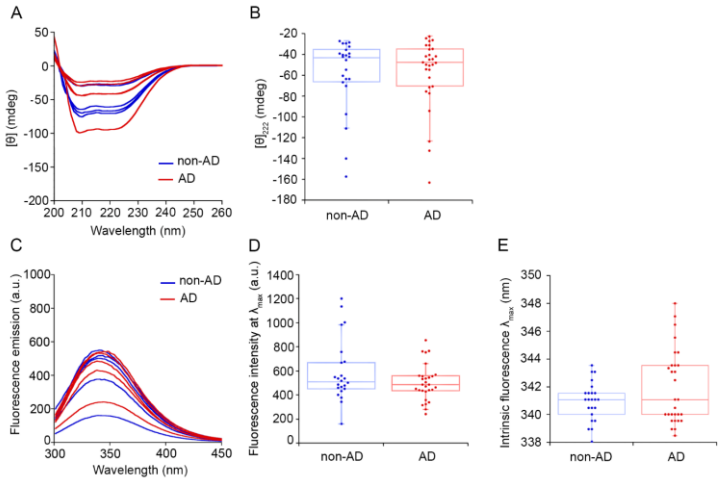

Figure 2.3 - Non-AD and AD CSFs have similar circular dichroism spectra and parameters. A) Far-UV CD spectra of five representative non-AD and five representative AD CSF

samples. B) Box plots reporting the ellipticity (θ) at 222 nm in all non-AD and AD CSF samples. C) Intrinsic fluorescence spectra of five representative non-AD and five representative AD CSF samples. D) Box plots reporting the fluorescence intensity at *λmax* in all non-AD and AD CSF samples. E) Box plots reporting the wavelength of maximum intrinsic fluorescence (*λmax*) in all non-AD and AD CSF samples. In panels B,D,E the boxes represent the central distributions of the individual points (from 25th to 75th percentile), the horizontal lines within the boxes are the median values, the whiskers are the range of values from the minimum to the maximum, excluding outliers, and the dots are individual experimental points.

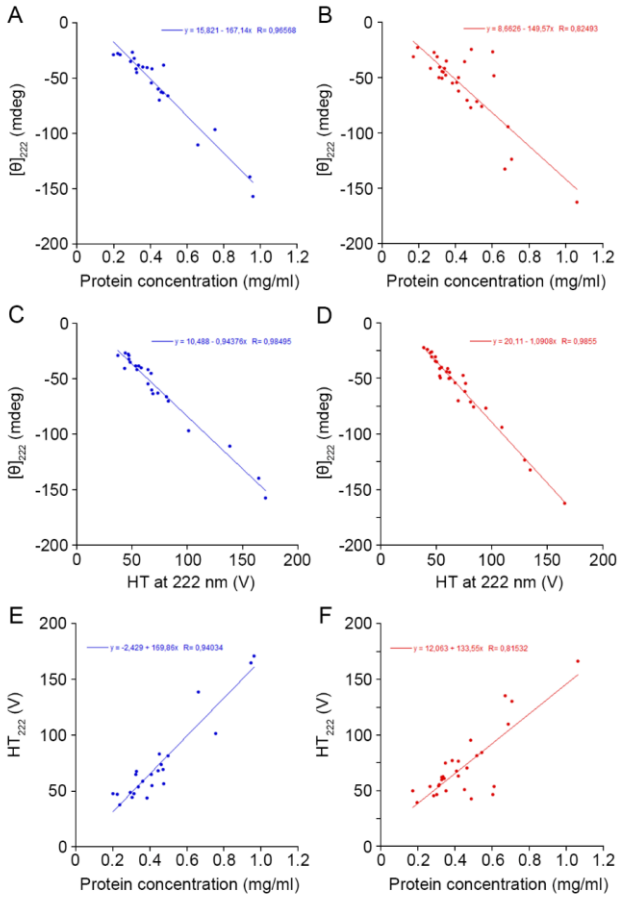

Figure 2.4 - Scatter plots reporting the dependence of θ_{222} on protein concentration, the dependence of θ_{222} on HT_{222} and the dependence of HT_{222} on protein concentration measured with the Bradford assay in non-AD and AD CSF samples. A-B) Scatter plots reporting the dependence of θ_{222} on protein concentration in non-AD A) and AD B) CSF samples. C-D) Scatter plots reporting the dependence of θ_{222} on HT_{222} in non- AD C) and AD D) CSF samples. D-E) Scatter plots reporting the dependence of HT_{222} on protein concentration measured with the Bradford assay in non-AD E) and AD F) CSF samples.

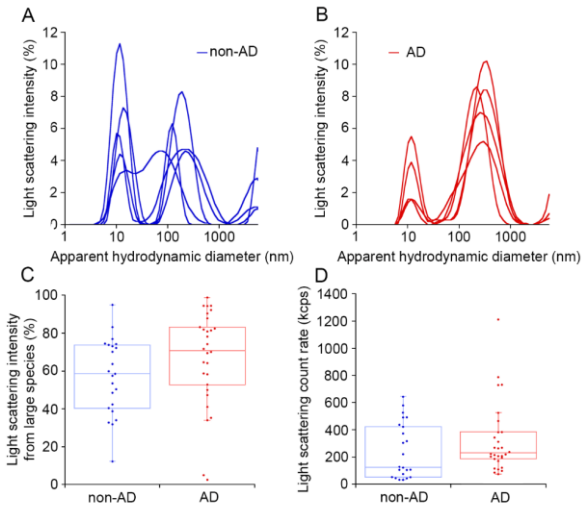

Figure 2.5 - Non-AD and AD CSFs have different quantities of protein aggregates. A-B) Size distributions by light scattering intensity (*LSI*) of particles present in five representative non-AD A) and five representative AD B) CSF samples acquired with DLS. C) Box plots reporting the *LSI* values from large species in all non-AD and AD CSF samples. D) Box plots reporting the light scattering count rate (*LSCR*) in all non-AD and AD CSF samples. The boxes, horizontal lines, whiskers and individual dots have the same meaning as in Figure 2a.

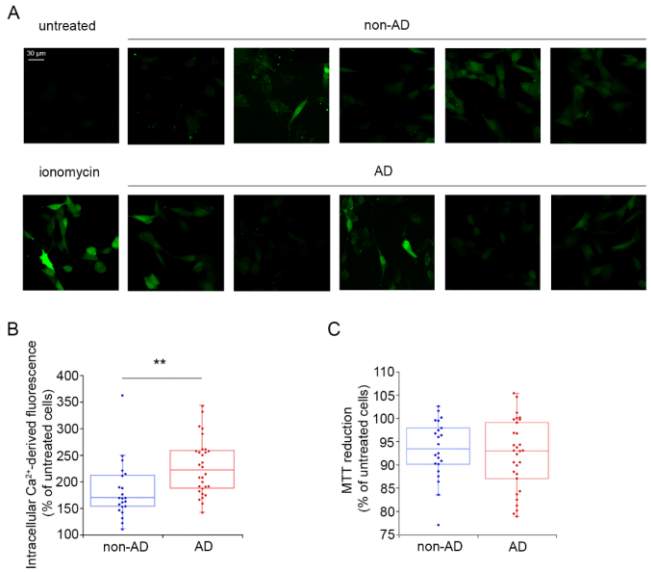

Figure 2.6 - Non-AD and AD CSFs have different abilities to destabilize cell membranes. A) Representative confocal microscope images showing the intracellular Ca^{2+} levels in SH-

SY5Y cells treated for 5 h with CSF samples of five non-AD and five AD patients. Untreated cells and cells treated with 1 μM ionomycin for 2 h are also shown as negative and positive controls, respectively. B) Box plots reporting the semi-quantitative analysis of all the Ca^{2+}-derived fluorescence values. C) Box plots reporting the MTT reduction values in SH-SY5Y cells treated for 24 h with CSF samples of all non-AD and all AD patients. The boxes, horizontal lines, whiskers and individual dots have the same meaning as in Figure 2a. The two populations were compared with the Student *t* test (** $p < 0.01$).

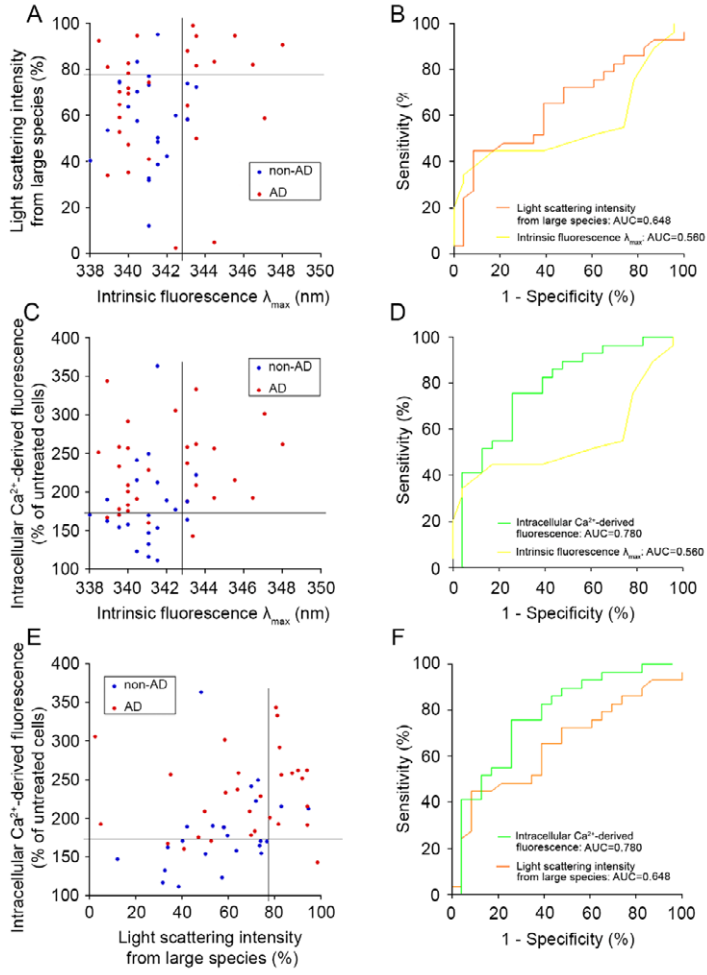

Figure 2.7 - Evidence for fluorescence, DLS, and toxicity parameters as potential AD biomarkers. A) Scatter plot for *LSI* from large protein species versus intrinsic fluorescence *λmax* with the optimized thresholds (*t**) derived from optimization of the Youden's indexes of the two parameters (horizontal and vertical lines, respectively). B) Corresponding ROC curves of the two parameters. AUC values are indicated for each parameter. C) Scatter plot for intracellular Ca^{2+} levels versus intrinsic fluorescence λ_{max} with the optimized thresholds (*t**) as horizontal and vertical lines, respectively. D)

Corresponding ROC curves of the two parameters. AUC values are indicated for each parameter. E) Scatter plot for intracellular Ca^{2+} levels versus *LSI* from large species with the optimized thresholds (t^*) as horizontal and vertical lines, respectively. F) Corresponding ROC curves of the two parameters. AUC values are indicated for each parameter. Non-AD (blue) and AD (red) CSF samples categorized to occupy the first quadrant (below both t^* values) or the remaining three quadrants (above at least one t^* value) provide a good separation between non-AD and AD patients.

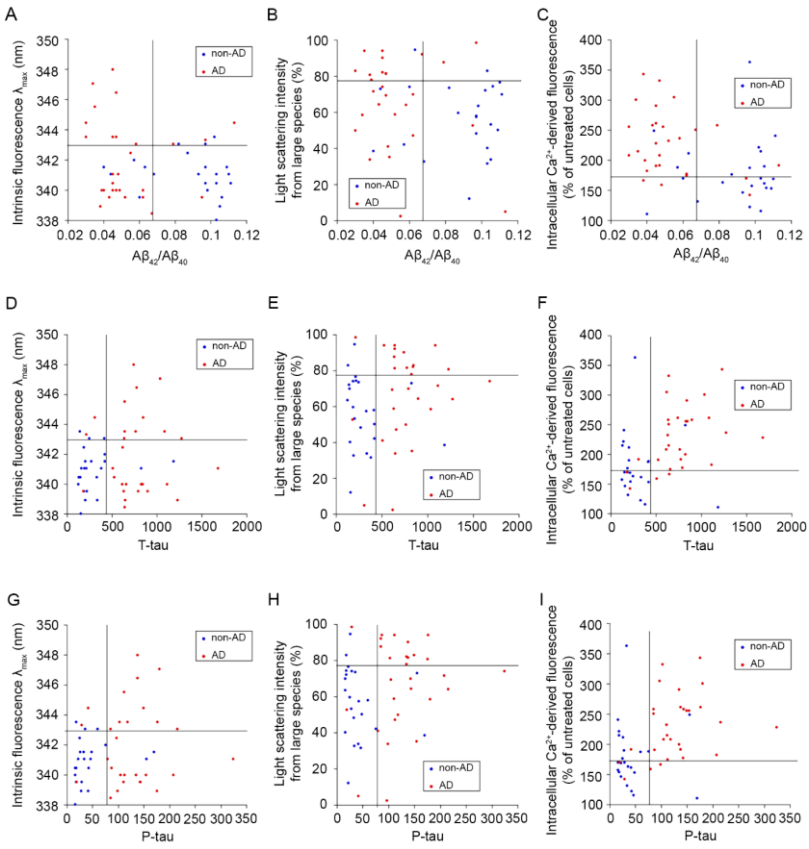

Figure 2. 8 - Comparison between novel and classical biomarkers. A,B,C) Scatter plots for intrinsic fluorescence *λmax* (A), *LSI* from large species (B) and intracellular Ca^{2+}-derived fluorescence (C) versus $A\beta_{42}/A\beta_{40}$ ratio. D,E,F) Scatter plots for intrinsic fluorescence *λmax* (D), *LSI* from large species (E) and intracellular Ca^{2+}-derived fluorescence (F) versus T-tau. G,H,I) Scatter plots for intrinsic fluorescence *λmax* (G), *LSI* from large species (H) and intracellular Ca^{2+}-derived fluorescence (I) versus P-tau. In all cases, the optimized thresholds (t^*) derived from optimization of the Youden's indexes of each couple of parameters are represented as horizontal and vertical lines, respectively. Non-AD (blue) and AD (red) CSF samples categorized to occupy the bottom-right quadrant or the remaining three quadrants (A-C), or the bottom-left quadrant or the remaining three quadrants (D-I) provide a good separation between non-AD and AD patients